Eur. Phys. J. D **22**, 269–277 (2003)
DOI: 10.1140/epjd/e2002-00245-5

THE EUROPEAN PHYSICAL JOURNAL D

Chaotic dynamics in a storage-ring free electron laser

G. De Ninno[1,2,a], D. Fanelli[3,b], C. Bruni[1,2], and M.E. Couprie[1,2]

[1] CEA, DSM/DRECAM/SPAM, CEA-Saclay, 91191 Gif-sur-Yvette, France
[2] LURE, bâtiment 209 D, Université de Paris-Sud, 91405 Orsay Cedex, France
[3] NADA, KTH, 10044 Stockholm, Sweden

Received 27 March 2002 / Received in final form 17 July 2002
Published online 21 January 2003 –

Abstract. The temporal dynamics of a storage-ring Free Electron Laser is here investigated with particular attention to the case in which an external modulation is applied to the laser-electron beam detuning. The system is shown to produce bifurcations as well as chaotic regimes. The peculiarities of this phenomenon with respect to the analogous behaviour displayed by conventional laser sources are pointed out. Theoretical results, obtained by means of a phenomenological model reproducing the evolution of the main statistical parameters of the system, are shown to be in a good agreement with experiments carried out on the Super-ACO Free Electron Laser.

PACS. 41.60.Cr Free-electron lasers – 05.45.Gg Control of chaos, applications of chaos

1 Introduction

Since its advent, the laser has evolved as a unique tool both for fundamental investigations and important applications in optical science and technology [1]. In providing coherent and intrinsically stable emission, lasers result fundamentally different from conventional light sources, which are characterised by a signal that is composite of random and uncorrelated emissions. Anyway, the view of the laser emission as an ordered and time-invariant process does not provide a full description of the whole picture. During the last twenty years, profound mathematical discoveries have revolutionised the understanding of nonlinear science. Lasers, in particular, have been found to exhibit a rich variety of nonlinear dynamical behaviours, including unstable or even chaotic regimes. As in the case of other nonlinear dynamical systems, the transition from stable to chaotic dynamics is obtained by varying a control parameter, such like the losses of the cavity [2], its optical length [3] or the gain of the amplification process [4]. The transitions are found to follow well-defined paths, regardless of the peculiar characteristics of the considered system. These universal "signatures" motivated both experimentalists and theoreticians in the search for physical systems exhibiting such phenomena, and in the investigation of their intrinsic similarity.

Concerning lasers, first experimental studies have been carried on a CO_2 laser [2,3]. It has been found that the modulation at a frequency f of the chosen control parameter may result not only in oscillations with frequency nf, being n an integer number, but also in a response at the sub-harmonics f/n. When the order n of the sub-harmonics grows indefinitely, the response of the laser becomes irregular, though the system remains deterministic. A quite impressive similitude has been remarked between the bifurcation diagram of the laser and that of the logistic map [5]. In order to reproduce these experimental results, a simple theoretical model has been used, resting on the dynamical interplay between the electromagnetic field within the optical cavity, and the variables of the material employed as "active medium". Theoretical work has been also done for demonstrating that the chaotic behaviour of a laser can be stabilised either by using a self-controlling feedback procedure [6,7] or by a further perturbation of a control parameter [8–11].

Experimental evidences of a close link with deterministic chaos has also been given in the pioneering work [4] for a kind of non-conventional laser source: a storage-ring Free Electron Laser (SRFEL).

After the first operation of a FEL in the infrared spectral range on a linear accelerator in 1977 [12], a second FEL was installed on the storage ring ACO and provided the first visible radiation in 1983 [13]. Present storage ring based FELs still supply the shortest FEL wavelength in the oscillator configuration (on ELETTRA [14]) and in the harmonic generation scheme on Super-ACO [15]. User applications performed since 1993 on the Super-ACO FEL have demonstrated the very good quality offered by such sources in terms of tuneability, high average power, rather short pulse duration and high degree of coherence [16]. These characteristics make, for example, the FEL very suitable for two colours experiments

[a] *Present address*: Sincrotone Trieste, 34012 Trieste, Italy.
[b] e-mail: `fanelli@nada.kth.se`

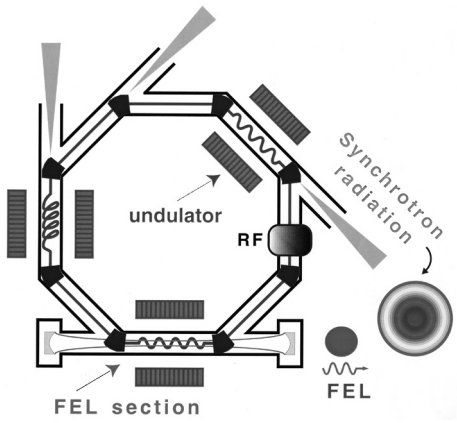

Fig. 1. Schematic layout of a SRFEL.

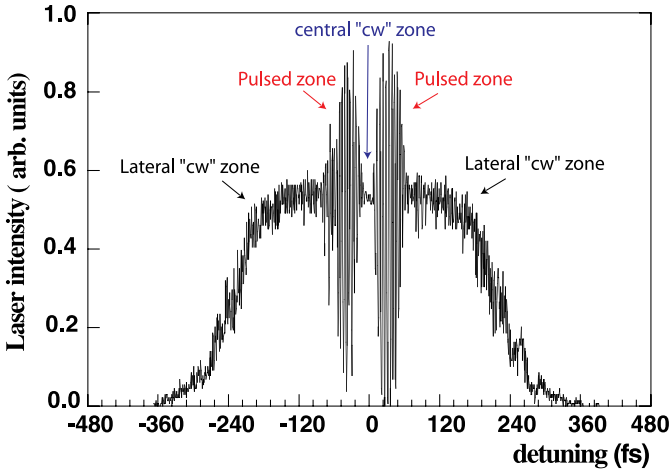

Fig. 2. A typical detuning curve (*i.e.* the laser intensity as a function of the laser-electron beam detuning amount) obtained for the case of the Super-ACO FEL operated in a configuration with only the main RF cavity. The synchronisation between the laser pulse and the electron bunch is changed by means of a modification of the RF frequency (a variation of 1 Hz inducing a laser-electron beam detuning of 1.2 fs). The employed experimental conditions are those reported in Table 1, with a total beam current of about 40 mA.

performed in combination with the naturally synchronised synchrotron radiation [17].

A SRFEL, the principle of which is shown in Figure 1, is a coherent source of radiation in which the active medium consists of an ultra-relativistic electron beam, moving in a periodic magnetic undulator. The alternating magnetic field forces the electrons to move along sine-like trajectories and, consequently, to emit radiation, known as spontaneous emission. Once stored in the optical cavity, the radiation is amplified to the detriment of the kinetic energy of the electrons. This process generally leads to the increase of the rms value of the particles energy (the so-called electron beam energy spread) and, as a consequence, to the reduction of the amplification gain, until this latter reaches the level of the cavity losses. Since it origins from synchrotron radiation, the SRFEL output presents a micro-temporal structure of the order of hundred of nanoseconds, which is determined both by the longitudinal dimension of the electron bunch and by the beam revolution period. On a larger (millisecond) temporal scale, the SRFEL dynamics depends strongly on the longitudinal overlap between the electron bunch(es) and the laser pulses at each pass inside the optical cavity (detuning condition). As it is shown in Figure 2 for the particular case of Super-ACO, a given detuning leads to a cumulative delay between the electrons and the laser pulses: the laser intensity may then appear "cw" (for a weak or strong detuning) or show a stable pulsed behaviour (for intermediate detuning) [14,18,19]. The narrow "cw" zone of the detuning curve (few ps around the perfect synchronism) is generally the most interesting for user applications. In fact, when in this zone, the laser is characterised by the maximum average power and the signal is the most close to the Fourier limit [20]. In order to keep the laser-electron beam synchronism and avoid the jittering, which could determine a migration towards one of the unstable, pulsed zones of the detuning curve, efficient feedback systems have been implemented on the Super-ACO [21] and UVSOR FELs [22]. SRFELs are complex, strongly coupled dynamical systems. The strong laser-electron beam coupling origins from the fact that, unlike a LINAC based Free Electron Laser, where the beam is renewed after each interaction, electrons are re-circulated. As a consequence, at every light-electron beam energy exchange, the system keeps memory of previous interactions.

The work that will be presented in this paper starts from the results obtained in 1990 on the Super-ACO FEL [4]. In the latter reference, it was experimentally shown that a periodic modulation at a given frequency f of the laser-electron beam detuning may lead to a period doubling of the laser intensity (*i.e.* to a laser response at a frequency $f/2$) or even to chaos for more important modulation amplitudes. Reference [4] contains also a first attempt to define the conditions (*i.e.* the amplitude and the frequency of the modulation) for which the bifurcation most likely occurs. The experimental data were discussed in connection with a simplified model based on a set of phenomenological rate equations, accounting for the coupled evolution of the laser intensity, of the electron-beam energy spread and of the gain of the amplification process. Such a model allowed to reproduce the basic features of the laser intensity evolution (in particular the saturation mechanism) only close to the perfect synchronism between the laser pulse and the electron bunch. This was a limiting factor for developing a comprehensive theoretical picture. In fact, the fundamental role played by the detuning has been only later understood: in [23] such effect has been shown to be responsible for the behaviour of the laser intensity ("cw" or pulsed) on the millisecond scale and to produce a further gain reduction over that induced by the increase of the electron-beam energy spread. The simple model presented in reference [23] was then improved by considering more accurately the evolution of the laser gain. This allowed to find a qualitative agreement between

experiments and numerical results, for the case of the Super-ACO FEL [24].

It is worth to stress that the loss of the laser-electron beam longitudinal overlapping may be induced by different phenomena such like a vibration of the cavity mirrors at the line frequency [25] or a modulation of the electron beam energy [26].

In this paper the model presented in [24] is used to get a deeper insight (with respect to that obtained in [4]) into the physics of deterministic chaos in a SRFEL. Numerical simulations are compared to a set of experiments performed on the Super-ACO FEL. In Section 2 the model is presented and shown to be able to reproduce quantitatively the observed features of the detuned FEL dynamics. Section 3 discusses the modifications induced to the dynamics by assuming an externally modulated detuning. Bifurcations are shown to occur for both the intensity and centroid position of the laser distribution. In Section 4 experimental results are presented. Finally, Section 5 contains concluding remarks and perspectives.

2 Theoretical model

The longitudinal dynamics of a SRFEL can generally be described by a system of rate equations accounting for the coupled evolution of the electromagnetic field and of the longitudinal parameters of the electron bunch [23].

The temporal profile of the laser intensity, y_n, is updated at each pass, n, inside the optical cavity according to:

$$y_{n+1}(\tau) = R^2 y_n(\tau - \epsilon)\,[1 + g_n(\tau)] + i_s(\tau), \qquad (1)$$

where τ is the temporal position with respect to the centroid of the electron bunch distribution; R is the mirror reflectivity; the detuning parameter ϵ is the difference between the electrons revolution period (divided by the number of bunches) and the period of the photons inside the cavity; i_s accounts for the spontaneous emission of the optical klystron[1]. The FEL gain $g_n(\tau)$ is given by:

$$g_n(\tau) = g_i \frac{\sigma_0}{\sigma_n} \exp\left[-\frac{\sigma_n^2 - \sigma_0^2}{2\sigma_0^2}\right] \exp\left[-\frac{\tau^2}{2\sigma_{\tau,n}^2}\right] \qquad (2)$$

where g_i and σ_0 are the initial (laser-off) peak gain and beam energy spread, while σ_n and $\sigma_{\tau,n}$ are the energy spread and the bunch length after the nth light-electron beam interaction. The first exponential in the right-hand side of equation (2) accounts for the modulation rate of the optical-klystron spectrum[2], while the second one reproduces the temporal profile of the electron bunch distribution. The bunch distribution is therefore assumed to keep its "natural" Gaussian profile under the action of the laser onset. This hypothesis entails that the interaction of the electron beam with the ring environment [30–32] is neglected. This important point will be further discussed with particular concern to the case of Super-ACO.

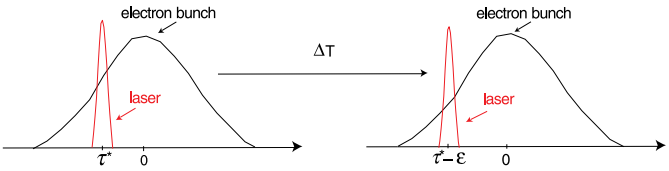

Fig. 3. Schematic layout of the pass-to-pass laser-electron beam interaction. ΔT stands for the period between two successive interactions, τ^* is the position of the laser centroid with respect to the peak of the electron density and ϵ accounts for the laser-electron beam detuning at each pass.

Defining $g_{n,0}$ as the peak gain after the nth interaction, $g_n(\tau)$ can be written in the form:

$$g_n(\tau) = g_{n,0} \exp\left[-\frac{\tau^2}{2\sigma_{\tau,n}^2}\right]. \qquad (3)$$

Figure 3 shows a schematic layout of the light-electron beam interaction in presence of a finite detuning ϵ.

The evolution of the normalised laser-induced energy spread $\Sigma_n = (\sigma_n^2 - \sigma_0^2)/(\sigma_e^2 - \sigma_0^2)$ is given by:

$$\Sigma_{n+1} = \Sigma_n + \frac{2\Delta T}{\tau_s}(I_n - \Sigma_n) \qquad (4)$$

where σ_e is the equilibrium value (*i.e.* that reached at the laser saturation) of the energy spread at the perfect tuning and ΔT is the bounching period of the laser inside the optical cavity; I_n is the normalised laser intensity defined as $I_n = (1/I_e)\int_{-\infty}^{\infty} y_n(\tau)\mathrm{d}\tau$ (being I_e the equilibrium value) and τ_s stands for the synchrotron damping time. Assuming that the saturation is achieved when the peak gain is equal to the cavity losses, P, the following relation holds[3]:

$$P = g_i \frac{\sigma_0}{\sigma_e} \exp\left[-\frac{\sigma_e^2 - \sigma_0^2}{2\sigma_0^2}\right]. \qquad (5)$$

By inserting equation (5) in equation (3) and recalling the definition of Σ_n, a closed expression for the peak gain is obtained:

$$g_{n,0} = g_i \frac{\sigma_0}{\sigma_n} \left[\frac{P}{g_i}\right]^{\Sigma_n} \left(\frac{\sigma_e}{\sigma_0}\right)^{\Sigma_n}. \qquad (6)$$

Note that in the derivation of equation (6) the variation of the bunch length during the FEL interaction has been taken into account. In this respect, the present model represents an improvement of the one proposed in [23], where

[1] The case of SRFELs implemented on an optical klystron is here considered [27,28]. An optical klystron consists of two undulators separated by a dispersive section, (*i.e.* a strong magnetic field) favoring the interference between the emission of the two undulators.

[2] The laser-off peak gain has been optimised by assuming $N + N_d = 1/(4\pi\sigma_0)$ in the expression of the modulation rate, where N is the periods' number of the undulators of the optical klystron and N_d is the interference order due to its dispersive section [29].

[3] As function of the cavity losses, the mirror reflectivity R is given by $\sqrt{1-P}$.

Table 1. Main parameters of the Super-ACO FEL operated with only the main (100 MHz) RF cavity.

The Super-ACO FEL	
Beam energy (MeV)	800
Laser-off bunch length $\sigma_{\tau,0}$ (rms, ps)	85
Laser-off beam energy spread σ_0	5.4×10^{-4}
Synchrotron damping time τ_s (ms)	8.5
Laser width at perfect tuning (ps)	20
Laser width at the maximum detuning (ps)	40
Laser wavelength (nm)	350
Pulse period (two bunches operation) ΔT (ns)	120
Laser-off peak gain g_i (%)	2.5
Cavity losses P (%)	0.5

the additional assumption $\sigma_n = \sigma_0$ in the definition of $g_{n,0}$ is made. A systematic numerical comparison allowed to show that this simplification may alter the period of the laser intensity in the pulsed regime, that is, as it will be shown in the next sections, a parameter of paramount importance for the study the laser response to an external modulation.

Figure 2 shows a typical detuning curve obtained for the case of the Super-ACO FEL operated with only the main radio-frequency (RF) cavity. The parameters characterising this configuration, which is the one of concern for the experiments reported in this paper, are listed in Table 1.

It is worth to mention that Super-ACO can be also operated making use of an additional RF (harmonic) cavity [33], which has been installed with the aim of improving the FEL performances. Its effect results in a shortening of the electron bunch. The consequent increase of the electron density leads to the enhancement of the gain of the amplification process. On the other hand, the interaction of the electron beam with the ring environment (*i.e.* the metallic wall of the ring vacuum chamber) is also reinforced. This leads to a degradation of the electron beam quality (*i.e.* "anomalous" increase of the laser-off bunch length *vs.* current and deformation of temporal beam distribution) limiting in part the beneficial effect of electron-density increase [34]. As regards the shape of the electron beam temporal distribution, the interaction with the ring vacuum chamber induces a perturbation of the "natural" Gaussian profile of the electron beam: the higher the cavity voltage, the stronger becomes the head-tail effect [35] deforming the electron distribution. It is worth to stress that, due to relative high value of the Super-ACO vacuum chamber impedance [36], the anomalous bunch lengthening and the perturbation of the beam profile are significant even when the harmonic cavity is passive. For the purpose of this paper, these perturbations can however be neglected in first approximation.

A quasi-symmetric beam profile reflects in a detuning curve that is almost symmetric for positive and negative

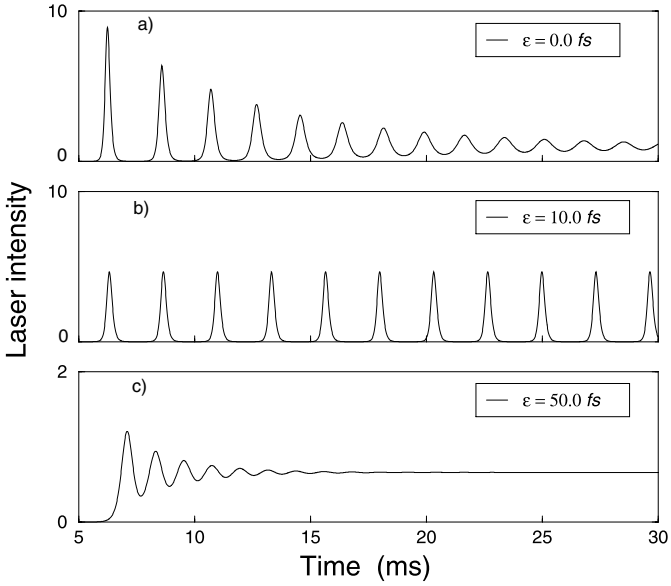

Fig. 4. Numerical results obtained by making use of the parameters listed in Table 1 and reproducing the different "natural" regimes of the laser intensity displayed in Figure 2. The "cw" regime in the nearly zero-detuning region (see a) is found to have an extension of (about) 10 fs (± 5 fs around the perfect tuning). The stable pulsed regimes, observed for an intermediate (positive and negative) detuning amount (see b), has an extension of (about) 35 fs. The lateral "cw" regimes (observed for large detuning values (see c), are found to have an extension of the order of few hundred of fs. Note that these theoretical findings reproduce quantitatively the experimental results reported in Figure 2. The laser intensity is normalised to the equilibrium value it reaches in the central "cw" zone of the detuning curve.

detuning amounts (see Fig. 2). The structure of the detuning curve has been studied by making use of the theoretical model presented above. The extension of the central ("cw") and lateral (pulsed) zones, which are the "playground" of the experiments that will be discussed in the next sections, has been found to be well reproduced (see caption of Fig. 4). Figure 4 shows the regimes of the laser intensity for different detuning amounts. Again, the numerical results have been found in quantitative agreement with experiments. Concerning, in particular, the pulsed regime, a careful experimental and numerical analyses [24] pointed out that the period of the laser-intensity oscillations is not a constant (as it has been implicitly assumed in [4]) but it is instead an almost linear function of the detuning amount.

The effect of an imperfect light-electron beam longitudinal overlapping also influences the equilibrium position of the laser centroid. As shown in Figure 5 [37], the laser position is quite sensitive to small detuning amounts, while it attains an almost constant value as the side zones of the detuning curve are approached.

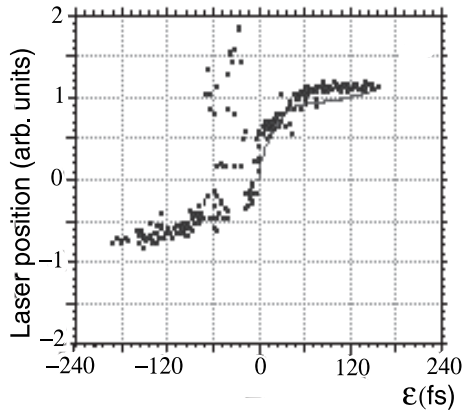

Fig. 5. Experimental behaviour of the position of the laser centroid with respect to the detuning amount ϵ. The employed experimental conditions are listed in Table 1.

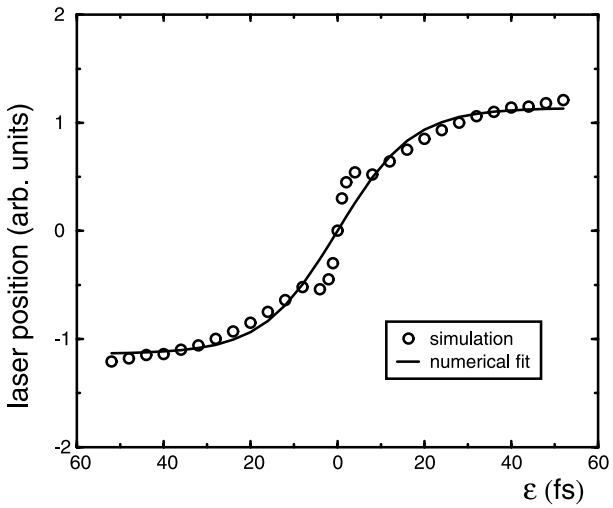

Fig. 6. Theoretical behaviour of the position of the laser centroid with respect to the detuning amount ϵ. Open circles refer to the simulations, while the solid line is obtained by making use of the fitting function $A\tanh(B\epsilon)$, with A, B free parameters.

Numerical simulations are in agreement with experiments (see Fig. 6) and allow to detail the interesting behaviour of the laser centroid in the close-to-zero detuning region.

3 Numerical simulations for modulated detuning

Consider now the modification induced to the system dynamics by the cumulative effect of an external periodic modulation applied to the detuning ϵ, namely:

$$\epsilon = a\sin(2\pi f t) + b, \tag{7}$$

where t represents the time elapsed, integer multiple of ΔT; f is the frequency of the oscillation, while the two amplitudes a and b control the maximum detuning amount. The oscillations are centered around b, being a the maximum elongation. Tuning the value of b, allows to explore the effects induced by the modulation in different zones. Simulations have been performed based on the model previously introduced, the main motivation being a systematic comparison with preliminary results of experiments carried on in Super-ACO. This point is addressed in the next section, where a brief description of the experimental set up is also reported. This paragraph is instead devoted to a more generally-oriented analysis, concerning the peculiar phenomena, that have been numerically found.

As already discussed in the previous section, several different regimes are produced in a SRFEL, for constant detuning amounts. For small ϵ the laser displays a "cw" intensity, while larger values of ϵ drive the system into stable oscillations. This "natural" pulsed regime is of paramount importance for the present study. The right boundary of the central, symmetric, "cw" zone will be labelled as ϵ_{th}.

Consider first the case for which b is set to zero. Hence, the average modulation is also zero. The external forcing, defined by equation (7), leads to a stable ($1T$) response only for small values of a, which prevent excursion of the modulated detuning outside the boundaries of the "cw" zone. When this excursion occurs, the modulation is generally found to induce a chaotic response of the laser intensity.

Quite different scenario is produced when b is set to some small value different from zero. This choice corresponds to introducing a slight asymmetry which, surprisingly enough, is responsible of a significant regularisation of the signal[4]. In Figure 7 the laser intensity is displayed as function of time, the upper panel being the modulation of ϵ. Simulations refer to a fixed value of the frequency while the amplitude is varied. The transition from a $1T$ to a $2T$ clearly occurs. It is worth stressing that the latter regime is observed for $a > \epsilon_{th}$.

In Figure 8 the laser intensity is plotted as function of time. Again, simulations refer to different values of a, while b and f are maintained constant. For small values of a, the laser response is locked to the frequency of the external modulation, thus displaying a $1T$ regime. For larger values the laser intensity passes through a chaotic region and, finally, attains a stable $3T$ regime.

In Figure 9 the position of laser centroid is represented, as function of time, for the same choice of parameters as in Figure 7. Oscillations are displayed and a transition from a $1T$ to $2T$ regimes is observed. This is, indeed, a quite general result: each time a bifurcation of the laser intensity takes place, an analogous response is observed for the position of the centroid.

Summing up, a wide number of distinct behaviours are recovered and, within them, bifurcations of both

[4] Note that this case can be considered more realistic than the previous one. In fact, even when the laser is operated as close as possible to the perfect tuning, a slight, uncontrollable, shift (corresponding to a b value of the order of one or two fs in the case of Super-ACO) has to be generally expected.

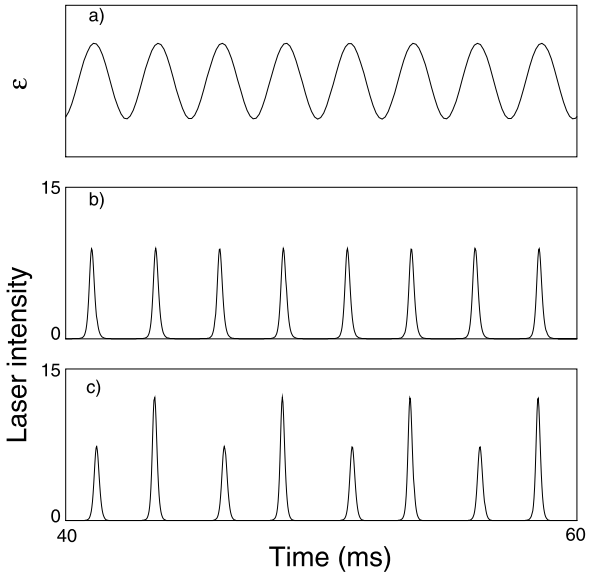

Fig. 7. Transition from a $1T$ to a $2T$ regime, for the laser intensity. Here $f = 400$ Hz and $b = 1$ fs. Figure (a) shows the modulation ϵ *versus* time. Figure (b) refers to $a = 19$ fs, while Figure (c) to $a = 34$ fs.

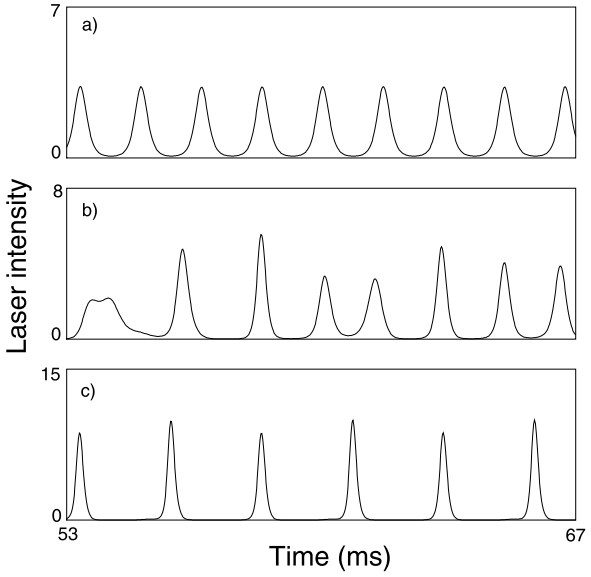

Fig. 8. Numerical simulations performed for $f = 600$ Hz. Figure (a) shows the laser intensity *vs.* time for $a = 10$ fs and $b = 2$ fs. The system is locked to the frequency of the external modulation, thus displaying a $1T$ regime. Figure (b) represents the laser intensity *vs.* time, for $a = 20$ fs and $b = 2$ fs. An a-periodic signal is found. In Figure (c), for $a = 30$ fs (and $b = 2$ fs), the system shows a $3T$ structure in qualitative agreement with experimental results of Figure 12.

intensity and centroid position of the laser, depending on the values of the parameters a and f. For $a < \epsilon_{th}$, *i.e.* when the oscillation is confined in the central "cw" zone of the detuning curve (few ps), the system is locked to the frequency imposed by the modulation and laser intensity exhibits regular oscillations of frequency f. As soon as the value of a exceeds the threshold ϵ_{th}, a "cascade"

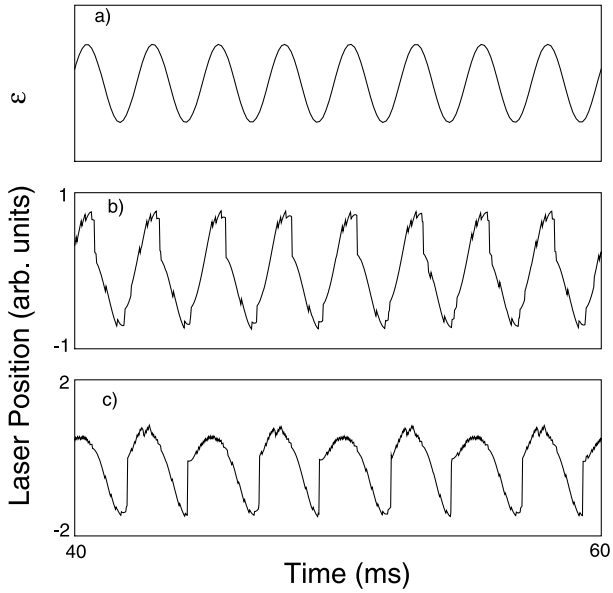

Fig. 9. Transition from a $1T$ to a $2T$ regimes, for the position of the laser centroid. Here $f = 400$ Hz and $b = 1$ fs, as in Figure 7. Figure (a) shows the modulation ϵ *versus* time. Figure (b) refers to $a = 19$ fs, while Figure (c) to $a = 34$ fs.

can occur. Therefore, one is led to conclude that excursions in the pulsed regime are a necessary requirement for the modulations to produce more complex behaviours. It is, in fact, believed that the observed periodic structures could be the result of the combined effect of the external and natural modulations. In addition, the system seems to be more sensitive to the natural frequencies (which, for the case of Super-ACO, lie between 400 Hz and 630 Hz), even though bifurcations have been detected outside this privileged range. These observations mark an important point of distinction with similar studies on conventional lasers, being the pulsed regime an intrinsic characteristic of the SRFEL.

Another interesting feature regards the value, $\hat{a}$, of the modulation amplitude for which the transition from $1T$ regime to more structured behaviours (*i.e.* $2T$, $3T$, ...) occurs. Numerically it has been observed that increasing the frequency, the value of $\hat{a}$ significantly decreases. This phenomenon, has been systematically observed in a wide range of frequencies (*i.e.* 200 Hz to 900 Hz). For larger values of f, the system is insensitive to the rapid external modulation, which therefore becomes ineffective.

Further, numerical simulations allowed to detect narrow windows, for which more complex periodic structures (*i.e.* $4T$, $5T$, $6T$, $8T$...) are displayed. Nervertheless, the existence of universal paths towards deterministic chaos remains an open issue.

Similar analysis have been carried out for larger values of b, such that the modulation is stably centred in one of the pulsed zones (see Fig. 10). This condition is achieved for small enough values of the amplitude a. Numerical results produce remarkably features, which will be commented in the following. As already pointed out in Section 2, the frequency of the oscillation in the pulsed

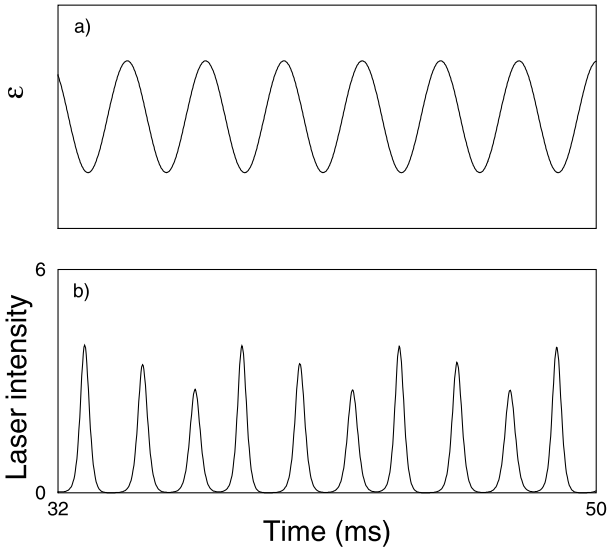

Fig. 10. (a) modulation ϵ *vs.* time. (b) Behaviour of the laser intensity. Here, $a = 2$ fs, $b = 25$ fs $f = 2/3, f_p = 381.6$ Hz. A $2T$ structure characterised by three peaks is displayed, in complete agreement with the prediction of relation (8).

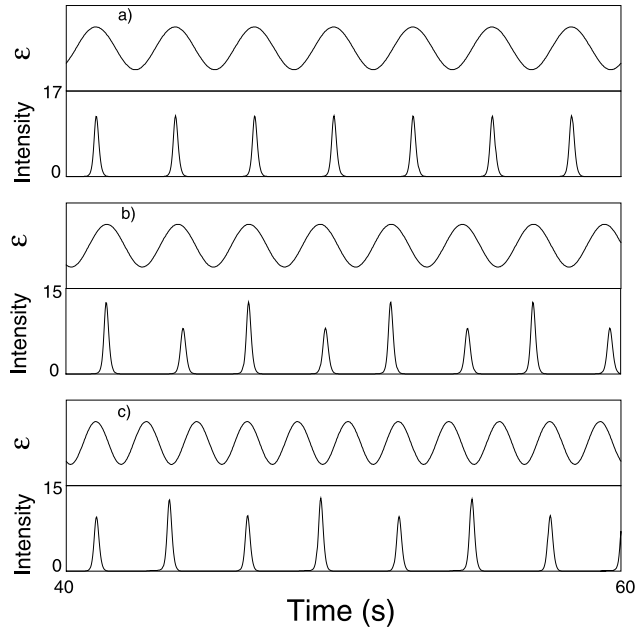

Fig. 11. Cascade $1T \rightarrow 2T \rightarrow 3T$, for laser intensity. Here $a = 37$ fs and $b = 2$ fs. From up to the bottom, the frequency are respectively 350 Hz (a), 390 Hz (b) and 550 Hz (c).

zone was shown to increase linearly with ϵ [24]. Assume f_p to be the frequency of the natural oscillation which is found for $\epsilon = b$, being $a = 0$. When the modulation of ϵ is switched on and the condition:

$$\frac{n}{f} = \frac{m}{f_p} \qquad n, m \in N, \quad n < m, \quad \frac{n}{m} \in Q \qquad (8)$$

is satisfied, the laser shows oscillations of frequency f/n, characterised by m peaks, spaced with period $2\pi/f_p$ (see Fig. 10, which refers to $n = 2$ and $m = 3$). Deviations are observed as (8) is progressively disattended (for instance, by slightly modifying the value of b). Note, however, that such behaviour occurs for discrete values of f, and is not maintained over a finite set of frequencies. Hence, its characterization in term of bifurcation is, somehow, stretched. Further experimental investigations will be addressed to validate these numerical findings.

Finally, an extensive campaign of simulations has also been performed varying the frequency f of the modulation, while keeping a fixed. A small value has been again assigned to the parameter b, in such a way that the center of the oscillations falls in the region of "cw" laser. A typical results is reported in Figure 11, where a cascade $1T \rightarrow 2T \rightarrow 3T$ is shown to occur. It is again worth to stress the crucial role that seems to be played by the pulsed zone.

4 Experimental results and their interpretation

Experiments have been performed by modifying the longitudinal overlap between the laser pulse and the electron bunch. This is done by modulating the radio-frequency in such a way that the variation of the detuning ϵ, in the form specified by equation (7), is achieved. Different results have been obtained by varying either the modulation amplitude (keeping f constant) or the modulation frequency (for fixed value of the amplitude of the modulation).

In Figure 12 the evolution of the laser intensity is investigated, when adopting the first procedure: f is set to a value close to the largest natural frequency. For small amplitudes of the modulation, a noisy $1T$ regime is observed. A transition toward a $2T$ response is produced when a is larger than ϵ_{th}, in qualitative agreement with the general picture outlined in the previous section. Larger values of a induce a chaotic response, before a stable $3T$ regime is attained (see Fig. 8, for a qualitative comparison).

In Figure 13, a $1T \rightarrow 2T$ transition is observed when varying the modulation frequency. Again, the bifurcation has been found to occur for an amplitude of the modulation large enough to drive the laser in the pulsed zone of the detuning curve. The transition is observed when f approaches the lowest natural frequency. This result is in a good agreement with the numerical simulations shown in Figure 11, which suggest that a further bifurcation $2T \rightarrow 3T$ could have been found, for larger frequencies. In addition, the frequency for which the transition is shown to occur, increases when the amplitude of the modulation is reduced (see Fig. 13). This result confirms the prediction of the theoretical analysis.

The response of the FEL to an external modulation of the laser-electron beam detuning has been also investigated by means of a double sweep streak camera. In particular in Figure 14, the occurrence of a period doubling of the laser centroid is detected.

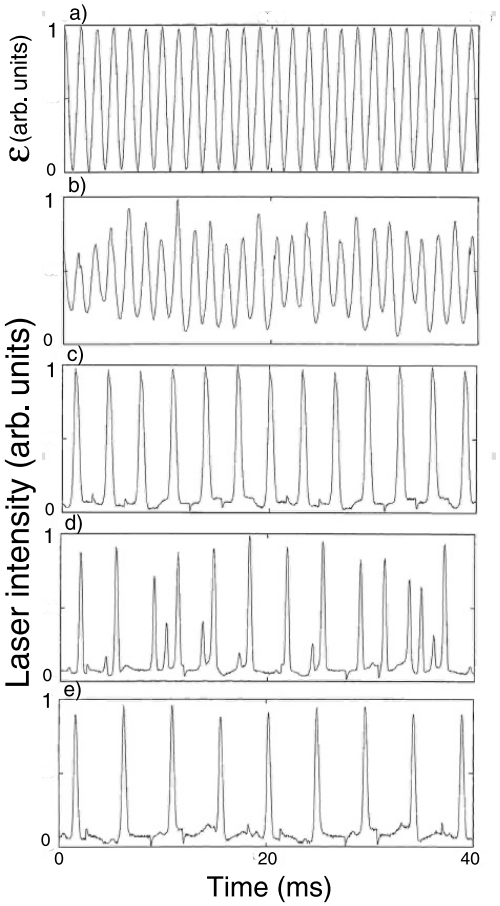

Fig. 12. Experimental response of the laser intensity to the detuning modulation. Here the $f = 660$ Hz. Figure (a) shows the modulation ϵ *versus* time. Figure (b) represents the laser intensity *vs.* time for $a = 7$ fs. The system system displays a (noisy) $1T$ regime. In Figure (c), for $a = 12$ fs, the laser intensity shows a $2T$ regime. In Figure (d), for $a = 20$ fs, an a-periodic signal is found. In Figure (e), for $a = 46$ fs, the laser intensity attains a stable $3T$ regime.

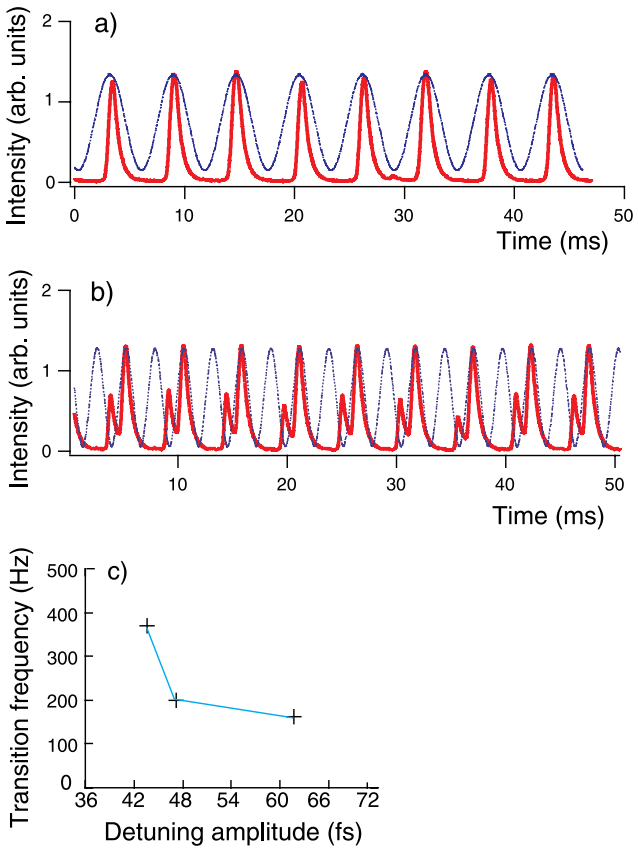

Fig. 13. Experimental response of the laser intensity to the detuning modulation. Here the amplitude $a = 36$ fs. Figure (a) shows the laser intensity *vs.* time (thick solid line) for $f = 174$ Hz. The thin solid line represents the detuning modulation (arbitrary units). The system displays a $1T$ regime. In Figure (b) the laser intensity (thick line) is represented *vs.* time, for $f = 377$ Hz. Again, the thin line refers to ϵ. A clear $2T$ response is found to occur. In Figure (c), the values of the frequency for which the system experiences the transitions from a $1T$ to a $2T$ regime, are plotted *vs.* the amplitude a. The decreasing tendency is clearly displayed.

5 Conclusions

A complete analysis of the dynamics of a SRFEL in presence of a longitudinal laser-electron beam detuning has been performed. Numerical simulations, based on the model presented in Section 2, and experimental results have been compared and shown to agree quantitatively, for a constant value of ϵ.

Further, the effect of an external modulated ϵ has been considered. The system has been shown to display bifurcations as well chaotic regimes for both the laser intensity and the position of its centroid, when either the amplitude or frequency of the modulation are tuned. Numerical analysis and preliminary experiments carried on for Super-ACO, agree in this respect. Moreover, a detailed series of simulations, over a wide range of values of the modulation parameters, allowed to point out the crucial role played by the naturally pulsed zones of the SRFEL detuning curve. This observation, confirmed by a careful analysis of the experimental data, seems to indicate that the link with analogous investigations for conventional lasers is not trivial, the pulsed regime being an intrinsic characteristic of the SRFEL.

In addition, conventional laser are shown to produce a complete cascade towards deterministic chaos, similar to that of the logistic map. In the case of SRFEL, experiments proved clearly the existence of $2T$ and $3T$ regimes, as well of chaotic behaviours. Nevertheless, a progressive increase of the periodicity of the structures ($1T$, $2T$, $3T$...) was not observed. Numerically, the interstitial regions laying between stable signals and chaotic regimes have been object of a detailed analysis. More complex periodic structures have been clearly detected ($4T$, $5T$, $6T$, $8T$...), even though, the attempt of identifying recurrent paths has, so far, failed. However, it is worthwhile stressing that the latter are shown to hold for a narrow range of tunability of the parameters. Hence, the transition from a low periodicity signal to chaos is generally sharp.

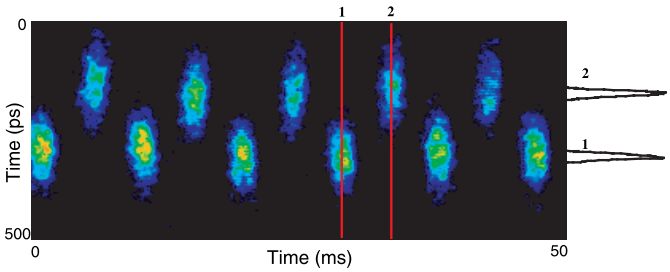

Fig. 14. Streak camera image of the Super-ACO FEL showing a $2T$ regime of the position of the laser centroid. The frequency is here $f = 250$ Hz and the modulation amplitude has been chosen large enough to exceed the central "cw" zone of the detuning curve. A vertical cut of the image provides the laser longitudinal distribution while on the horizontal axis one can follow the evolution in time of the distribution profile.

The theoretical part of this work, described in Sections 2 and 3 above, was done by G.D.N. and D.F. These authors contributed equally to this part of the work. The experimental part, described in Section 4 above, was done by C.B. and M.E.C. We thank M. Billardon, P. Glorieux and D. Dangoisse for stimulating discussions. We gratefully acknowledge the help of D. Garzella, D. Nutarelli S. Randoux, R. Roux and B. Visentin for carrying on experiments. We also thank E. Aurell for a careful reading of the manuscript. The work of D.F. was supported by the Swedish Research Council through grant NFR F 650-19981250. Financial support to the work of G.D.N. was provided by the TMR contract N ERB 4061 PL 97-0102.

References

1. A. Hall, J. Jakson, *The Physics and technology of Laser Resonators* (Adam Hilger editor, 1989)
2. F.T. Arecchi *et al.*, Phys. Rev. Lett. **49**, 1217 (1982)
3. T. Midavaine, D. Dangoisse, P. Glorieux, Phys. Rev. Lett. **55**, 1989 (1985)
4. M. Billardon, Phys. Rev. Lett. **6**, 713 (1990)
5. C. Beck, F. Schlogl, *Thermodynamics of chaotic systems* (Cambridge University Press, Cambridge, 1993)
6. V. Petrov *et al.*, J. Chem. Phys. **96**, 7503 (1992)
7. S. Bielawski *et al.*, Phys. Rev. E **49**, 971 (1994)
8. R. Lima, M. Pettini, Phys. Rev. A **41**, 726 (1990)
9. A. Azevedo, M. Rezende, Phys. Rev. Lett. **66**, 1342 (1991)
10. Y. Liu, R. Leite, Phys. Lett. A **185**, 35 (1994)
11. E. Ott *et al.*, Phys. Rev. Lett. **64**, 1196 (1990)
12. D.A.G. Deacon *et al.*, Phys. Rev. Lett. **38**, 892 (1977)
13. M. Billardon *et al.*, Phys. Rev. Lett. **51**, 1652 (1983)
14. M. Trovo *et al.*, Nucl. Instr. Meth. A **483**, 157 (2002)
15. R. Prazeres *et al.*, IEEE **27**, 1061 (1991)
16. M.E. Couprie *et al.*, Rev. Scient. Inst. **65**, 1485 (1994)
17. M. Marsi *et al.*, Appl. Phys. Lett. **70**, 895 (1997)
18. M.E. Couprie *et al.*, Nucl. Instr. Meth. A **331**, 37 (1993)
19. H. Hama *et al.*, Nucl. Instr. Meth. A **375**, 32 (1996)
20. M.E. Couprie *et al.*, Nucl. Instr. Meth. A **475**, 229 (2001)
21. M.E. Couprie *et al.*, Nucl. Instr. Meth. A **358**, 374 (1995)
22. M. Hosaka *et al.*, Nucl. Instr. Meth. A **445**, 208 (2000)
23. M. Billardon, D. Garzella, M.E. Couprie, Phys. Rev. Lett. **69**, 2368 (1992)
24. G. De Ninno, D. Fanelli, M.E. Couprie, Nucl. Instr. Meth. A **483**, 177 (2002)
25. M. Hosaka *et al.*, Nucl. Instr. Meth. A **445**, 208 (2000)
26. G. Dattoli *et al.*, IEEE J. Quant. Electr. **34**, 1782 (1998)
27. N.A. Vinokurov *et al.*, `Preprint INP77.59`, Novossibirsk, unpublished
28. P. Elleaume, J. Phys. (Paris) **45**, 997 (1984)
29. P. Elleaume, J. Phys. (Paris) **44**, 1 (1983)
30. G. Dattoli, A. Renieri, Nucl. Instr. Meth. A **375**, 1 (1996)
31. M. Migliorati, L. Palumbo, Nuovo Cim. A **112**, 461 (199)
32. H. Hama *et al.*, Nucl. Instr. Meth. A **341**, 1 (1994)
33. M. Billardon *et al.*, Proceedings EPAC conference, Stockholm, Sweden, 1998
34. R. Roux *et al.*, Phys. Rev. E **58**, 6584 (1998)
35. G. Dattoli *et al.*, Phys. Rev. E **58**, 6570 (1988)
36. G. Dattoli *et al.*, Nucl. Instr. Meth. A **471**, 403 (2001)
37. D. Garzella *et al.*, Nucl. Instr. Meth. A **341**, 24 (1994)
38. D. Dangoisse, P. Glorieux, D. Hennequin, Phys. Rev. A **36**, 4775 (1987)